The E3 ligase MARCH5 is a PPARγ target gene that regulates mitochondria and metabolism in adipocytes

Running title: MARCH5 regulates adipocyte metabolism

Simon T. Bond[1], Sarah C. Moody[1], Yingying Liu[1], Mete Civelek[2], Claudio J. Villaneuva[3], Paul Gregorevic[1], Bronwyn A. Kingwell[1], Andrea L. Hevener[2], Aldons J. Lusis[2], Darren C. Henstridge[1], Anna C. Calkin[1,4], Brian G. Drew[1,4#]

1. Baker Heart & Diabetes Institute, Melbourne, Victoria, Australia, 3004.
2. University of California, Los Angeles, CA 90095, USA
3. University of Utah, Salt Lake City, UT 84132, USA
4. Central Clinical School, Monash University, Melbourne, Australia, 3004

Corresponding Author

Corresponding Author Details:
Dr Brian G. Drew
Email: brian.drew@baker.edu.au
Baker Heart & Diabetes Institute
PO Box 6492, St Kilda Road Central
VIC, Australia, 3004

Keywords:
March5, mitochondria, adipose tissue, PPAR-gamma, lipid metabolism

Abstract

Mitochondrial dynamics refers to the constant remodelling of mitochondrial populations by multiple cellular pathways which help maintain mitochondrial health and function. Disruptions to mitochondrial dynamics often leads to mitochondrial dysfunction, which is frequently associated with disease in rodents and humans. Consistent with this, obesity is associated with reduced mitochondrial function in white adipose tissue, partly via alterations in mitochondrial dynamics. Several proteins are known to regulate mitochondrial dynamics including the E3 ubiquitin ligase MARCH5; however, the role of these proteins in adipocytes has been poorly studied. Here, we show that MARCH5 is regulated by PPARγ during adipogenesis and is correlated with fat mass across a panel of genetically diverse mouse strains, in *ob/ob* mice, and in humans. Furthermore, manipulation of MARCH5 expression both *in vitro* and *in vivo* alters mitochondrial function, affects cellular metabolism and leads to differential regulation of several metabolic genes. Thus, our data demonstrate a link between mitochondrial dynamics and metabolism which defines MARCH5 as a critical link between these interconnected pathways.

Introduction

Mitochondria are essential organelles whose primary role in mammalian cells is to generate cellular energy. However, they also have crucial roles in maintaining processes such as calcium signalling, cell growth and division, apoptosis and cell death (23). Historically, the bulk of studies investigating mitochondrial disease have been performed in tissues of high energy demand, including striated muscles and the brain. However, more recent studies have also demonstrated that manipulating mitochondrial health and activity in adipose tissue can have profound effects on adipose tissue expansion and differentiation, a process largely regulated by the nuclear receptor peroxisome proliferator-activated receptor gamma (PPARγ) (35). PPARγ is the master regulator of adipogenesis and consequently modulates several gene sets necessary for adipocyte function, including those involved in mitochondrial homeostasis (40, 41). Indeed, the thiazolidinediones or TZDs such as pioglitazone, which are indicated for type 2 diabetes in humans, are ligands for PPARγ and have been shown to have beneficial effects on adipose tissue expansion and mitochondrial activity in individuals with obesity and type 2 diabetes (T2D) (6, 22).

Mitochondrial integrity is fundamental to maintaining healthy cellular functions. Indeed, when mitochondria become dysfunctional or damaged, overall cellular health deteriorates which can induce apoptosis and cell death (18, 27, 30, 46). Mitochondria continually divide and fuse through well described mechanisms of fission (fragmentation) and fusion (elongation) to regulate mitochondrial health, including the removal of dysfunctional and unhealthy mitochondria through mitophagy (11, 13, 19).

These processes, collectively known as mitochondrial dynamics, are part of a highly regulated and co-ordinated program which sees mitochondria enter a constant state of flux through processes such as biogenesis, fusion, fission and mitophagy (1, 13). Several key proteins have been identified to regulate mitochondrial fission and fusion including dynamin-1-like protein (Drp1), dynamin-like 120kDa protein (optic atrophy 1-OPA1), and mitofusins 1 and 2 (Mfn1/2) (8, 44). Mitochondrial dynamics is also important in maintaining the health of white adipose tissue (WAT), as studies have shown that inhibition of autophagy or mitophagy results in a severe reduction in WAT mass reminiscent of lipodystrophy (10, 32, 47). Improving mitochondrial health by increasing mitochondrial function has the potential to restore or improve the function of WAT. This was elegantly highlighted by Scherer and colleagues, who demonstrated substantial improvement in metabolic health in a mouse model of obesity that specifically overexpressed the protein MitoNEET in adipose tissue (12).

Another protein more recently implicated in mitochondrial dynamics is Membrane Associated Ring-CH-Type Finger 5 (MARCH5) (3, 20, 37). The MARCH family of proteins are RING type transmembrane E3 ubiquitin ligases that regulate a range of cellular processes by ubiquinating target proteins and facilitating their degradation (28). MARCH5 is the only member of the MARCH family localised to the mitochondria where it is bound to the outer mitochondrial membrane (OMM) with the active E3 ligase domain protruding into the cytosol. MARCH5 has been implicated in the regulation of a variety of cellular processes including apoptosis, viral signalling, endoplasmic reticulum-mitochondria binding and calcium dynamics. However, the most well documented role for MARCH5 is its ability to ubiquitinate and regulate several mitochondrial dynamics

94 proteins including Drp1, Mfn1/2, mitochondrial fission 1 protein (Fis1) and mitochondrial
95 dynamics proteins 49 & 51kDa (Mid49/51) (3, 33, 42, 43) . Furthermore, recent studies
96 have demonstrated that MARCH5 is a regulator of hypoxia induced apoptosis and
97 mitophagy via the ubiquitination of the mitochondrial receptor FUN14 domain-containing
98 protein 1 (FUNDC1), demonstrating a further link between MARCH5 and mitophagy
99 pathways (2). To date, most studies on MARCH5 have been performed in neuronal
100 cells and tissues, and there has been no investigations into the role of MARCH5 in
101 metabolic tissues including adipose tissue. Thus, the current study aimed to investigate
102 the role of MARCH5 in adipose tissue. We provide *in vitro* and *in vivo* evidence that
103 MARCH5 expression is enriched in adipose tissue and is regulated by PPARγ, and that
104 modulation of MARCH5 in adipocytes regulates energy metabolism.

Results

MARCH5 expression is reduced in obesity and correlates with PPARγ expression. Initially, we aimed to determine if MARCH5 expression was correlated with measures of adiposity and obesity in mice and humans. Thus, we analysed data from a collection of genetically diverse mouse strains known as the hybrid mouse diversity panel (HMDP), that has demonstrated utility in identifying genetic drivers of complex traits (25, 26, 31). We explored data from the HMDP microarray expression profiles to analyse *March5* transcript expression in white adipose tissue (WAT) across 101 strains of HMDP mice fed a HFD (25). The heat map in Figure 1A, demonstrates that *March5* mRNA expression is strongly negatively correlated with several indices of adiposity including fat mass, percent body fat and the weight of multiple fat pads including retroperitoneal (RFP), gonadal (GFP), subcutaneous (FFP) and mesenteric (MFP) (Fig 1A & 1B). These data also confirm that the majority of adiposity measurements in the HMDP strains positively correlate with each other, and with indices of metabolic dysregulation (plasma glucose and insulin levels), accurately replicating known phenotypes associated with metabolic syndrome. Consistent with MARCH5 being a mitochondrial protein and reduced in the setting of increased adiposity, we also reveal that several other mitochondrial genes (*Dnm1l*, *Mff*, *Opa1*, *Rhot1* and *Mfn1*) were negatively correlated with fat mass in the HMDP (Table 1). Additionally, to validate this interaction in an experimental model of obesity, we analysed *March5* expression in WAT of male C57Bl/6J and *ob/ob* mice, which further demonstrated that *March5* expression was reduced in the setting of increased adiposity (Fig 1C)

Given this correlation between *March5* and fat mass in rodent models, we next sought to determine whether *March5* expression was also decreased in association with increasing adiposity in humans. Subsequently, we analysed the expression of *March5* in abdominal subcutaneous adipose tissue biopsies from participants in the METSIM Study (770 participants across a range of obesity indices (4). These data demonstrate a significant negative correlation of *March5* with fat mass ($r= -0.202$, $p=9.75e^{-9}$), consistent with data from the HMDP strains and confirming that *March5* expression is negatively correlated with adiposity in both mice and humans (Fig 1B, 1D). Finally, in order to validate correlation data from the human METSIM study, we performed Western blot analysis on subcutaneous WAT biopsies collected from a small cohort of age-matched male participants across lean and obese groups (52.8±10.8 vs 54.2±8.4 years old, respectively). These data demonstrate that those in the obese group (BMI=33.0±4.2kg/m^2) with subsequently impaired fasting blood glucose levels (iFBG = 9.9±3.3 mmol/L), had a lower abundance of PPARγ and MARCH5 protein in their WAT compared with lean individuals (lean = 25.3±3.3kg/m^2), who were normal glucose tolerant (NGT = 5.0±0.4 mmol/L), confirming that MARCH5 is reduced in the setting of obesity and metabolic dysregulation, further suggesting that pathways important to adipocyte expansion are also downregulated in obesity (Fig 1E-G). Collectively, these data demonstrate that MARCH5 expression has a strong negative relationship with fat mass in both rodents and humans, and that pathways associated with adipogenesis (PPARγ) and mitochondrial function are co-ordinately down regulated in WAT in the setting of obesity.

MARCH5 expression correlates with PPARγ and is a likely PPARγ target gene. To investigate whether MARCH5 and PPARγ expression are co-ordinately regulated as suggested by data in Figure 1, we again probed microarray datasets from WAT in the HMDP mouse strains. Figure 2A plots transcripts in WAT that positively correlated (r>0.4) with *Pparg* gene expression across all strains of the HMDP mice. Several well described PPARγ target genes were strongly positively correlated with *Pparg* expression in this analysis (red dots) including *Hibadh*, *Pex13*, *Osbpl11* and *β-Klotho*. Interestingly, the most strongly correlated transcript with *Pparg* was *March5* (blue circle and arrow, Fig 2A). These data demonstrate that correlation analysis is a useful approach to identify PPARγ regulated genes, which implicated *March5* as a PPARγ target gene. To provide further evidence for this, we performed pathway enrichment analysis of all transcripts that positively correlated with *Pparg* at a mid-weight bicorrelation (bicor) cut-off of r>0.5, equating to 173 individual genes (Table 2). This analysis displayed strong enrichment for pathways including mitochondria, peroxisome and lipid/fatty acid metabolism (Fig 2B), consistent with pathways classically regulated by PPARγ and supporting the notion that this gene set is indeed reflective of PPARγ transcriptional activity.

Considering that *March5* was strongly correlated with PPARγ expression in WAT, we performed further experiments to investigate its tissue distribution in mice. MARCH5 protein levels were robustly detected in both brown adipose tissue (BAT) and gonadal WAT in C57BL/6J mice as shown by Western blot analysis (Fig 2C). Furthermore, qPCR analysis of several tissues from male WT mice demonstrated that *March5*

expression was enriched in WAT and BAT compared to other tissues such as heart, skeletal muscle and liver (Fig 2D), consistent with *March5* being a transcriptional target of PPARγ. To directly test whether *March5* was a transcriptional target of PPARγ and regulated by the adipogenic transcriptional program, we analysed existing PPARγ, RXRα and C/EBPα ChIP-Seq datasets from differentiating adipocytes and investigated whether these pro-adipogenic transcription factors (TFs) were enriched on the *March5* locus (14, 16). These data confirm that all three TFs occupied the *March5* promoter in close proximity to the transcriptional start site (TSS) (Figure 2E), confirming that PPARγ, RXRα and C/EBPα co-operatively regulate the expression of *March5*, similar to that shown for other adipogenic genes (16). These findings are strengthened by data shown in figures 2F & 2G, which present findings from primary adipocytes isolated from WT and adipocyte specific PPARγ-KO mice (PPARγ floxed [WT] and PPARγ floxed + aP2 Cre [PPARγ-KO], respectively). These data confirm that WT adipocytes differentiated proficiently, however consistent with the known role of PPARγ in adipogenesis, PPARγ-KO adipocytes had a severely impeded ability to differentiate. In WT adipocytes, *March5* expression was upregulated upon differentiation, however this effect was completely blunted in PPARγ-KO differentiated cells, and was also lower in undifferentiated PPARγ-KO cells. Thus, the data presented above provide compelling evidence that *March5* is transcriptionally regulated by PPARγ and the adipogenic program, and is subsequently highly enriched in adipose cells and tissue *in vitro* and *in vivo* respectively.

Mitochondrial proteins including MARCH5 are upregulated during adipocyte differentiation. Given several studies have demonstrated that MARCH5 influences proteins which regulate mitochondrial dynamics including Mfn2 and Drp1 (9, 16, 20), we investigated this pathway in our own experimental models. Accordingly, we performed Western blotting in immortalised MEFs isolated from WT and MARCH5-KO mice and demonstrated that loss of MARCH5 in these cells promotes an increase in Mfn2 protein abundance (Fig 3A). This is consistent with other studies which have demonstrated that Mfn2 is ubiquinated by MARCH5 and subsequently degraded, thereby promoting an environment that would induce mitochondrial fusion (20, 33).

We also determined whether MARCH5 was regulated in adipocytes independently of other mitochondrial proteins, or whether it was part of a global mitochondrial change in differentiating adipocytes as eluded to above. To investigate this, we performed immunoblotting of proteins from WT 3T3-L1 adipocytes at different stages of adipocyte differentiation (pre-diff, day 0, day 1, day 3, day 6 and day 10). Figures 3B & 3C confirm that MARCH5, Drp1 and Mfn2 increased substantially in adipocytes from day 3 of differentiation, which coincided with an increase in PPARγ2 expression (the adipocyte specific variant - upper band). Furthermore, other mitochondrial proteins were also increased at this time point including proteins of the electron transport chain (complex II-V) and Porin (*Vdac1*). These findings are consistent with PPARγ and adipocyte differentiation promoting an upregulation of genes related to increasing mitochondrial activity, including an increase in MARCH5. Because we show that MARCH5 is increased in differentiating adipocytes, and that MARCH5 deletion leads to an increased

abundance of Mfn2, we wanted to determine if MARCH5 could play a key role in regulating adipocyte mitochondrial fusion, metabolism and lipid storage.

Manipulating MARCH5 abundance in 3T3-L1 adipocytes regulates mitochondrial respiration and glycolysis. In order to investigate the functional effect of MARCH5 in differentiating adipocytes, we generated stable MARCH5 knockdown (shMARCH5) and control knockdown (shLuc) 3T3-L1 adipocytes using lentiviral delivered shRNAs. Figure 4 confirms an average 50% knockdown of *March5* at various stages of differentiation (Fig 4A), with nearly 80% reduction in the early stages of differentiation, the critical time point we demonstrate that MARCH5 sharply increases in WT cells. Figure 4 also shows that depletion of MARCH5 in 3T3-L1 adipocytes had no effect on expression of genes involved in adipocyte differentiation and mitochondrial dynamics including *Pparg* (Fig 4B), *Dnm1L* (Fig 4C) and *Mfn2* (Fig 4D). Despite observing no change in *Dnm1L* and *Mfn2* gene expression, we and others have demonstrated that MARCH5 is an upstream protein regulator of the outer mitochondrial fusion protein Mfn2. To determine if depletion of MARCH5 in 3T3-L1 adipocytes modulated mitochondrial fusion, we stained MARCH5 knockdown and control cells with MitoTracker Deep Red and performed confocal microscopy. Mitochondrial populations in MARCH5 knockdown adipocytes were observed to be elongated and networked compared with fragmented mitochondria in control cells (Fig 4E), which was significant upon quantification (Fig 4F), confirming that depletion of MARCH5 in adipocytes promoted a pro-fusion phenotype. Moreover, western blotting for Mfn2 was also observed to be elevated in *March5* depleted cells (Fig 4G), providing further evidence of a pro-fusion phenotype in these cells.

Because of the tight associations between mitochondrial function and energy metabolism, we investigated whether MARCH5 knock-down and control adipocytes had altered substrate storage and utilisation. Although MARCH5 depletion promoted mitochondrial fusion, Oil Red O staining for neutral lipid abundance did not show a significant difference in the MARCH5 depleted cells (Fig 4H, 4I). Furthermore, we also demonstrated that both basal and insulin stimulated glucose uptake was approximately 2-fold higher (5168±715 vs 9124±1814 cpm/mg and 10293±1127 vs 17191±612 cpm/mg, $p<0.05$) in MARCH5 knockdown cells, suggesting that depletion of MARCH5 led to an increased reliance on carbohydrate metabolism (Fig 4J).

Finally, because of the observed effects on mitochondrial fusion and apparent preference for carbohydrate metabolism, we investigated metabolic parameters and mitochondrial function using the Seahorse Flux Analyser. The Seahorse apparatus provides measures of cellular oxygen consumption rate (OCR - surrogate readout of oxidative phosphorylation) and extracellular acidification rate (ECAR – surrogate readout of glycolysis). Our data demonstrated that MARCH5 knockdown in adipocytes increased basal mitochondrial respiration as indicated by an increased basal OCR, which coincided with an increase in ATP linked respiration (Fig 4L). In addition, MARCH5 knockdown adipocytes had increased rates of glycolysis (Fig 4M) compared with control cells, further suggesting that MARCH5 depletion modulates glucose metabolism and subsequently increases mitochondrial metabolism. This is effect on glycolysis was also supported by qPCR data demonstrating that depletion of MARCH5 increases the expression of the glycolytic enzyme *Pyruvate dehydrogenase kinase*

(*Pdk4*) (Fig 4K), consistent with observed increases in ECAR measured by the Seahorse.

In light of the results observed for MARCH5 depletion in adipocytes, we sought to determine whether reciprocal effects would be observed following overexpression of MARCH5. This was achieved by infecting differentiated 3T3-L1 cells with adenoviruses that express MARCH5 or a control protein (GFP). Following adenoviral transduction, robust expression of (Fig 4N) *Gfp* and (Fig 4O) *March5* mRNA was demonstrated at day 7 post differentiation (1±0.1 vs 0±0.0 fold change and 2±1.5 vs 72±5 fold change relative to *Gfp* expression, respectively, $p<0.05$). Using qPCR and the Seahorse analyser we revealed that differentiated 3T3-L1 cells overexpressing MARCH5 had reduced *Pdk4*, basal respiration and glycolysis compared with cells overexpressing GFP, however these cells still retained the capacity to increase mitochondrial respiration following FCCP stimulated mitochondrial uncoupling (Fig 4P, 4Q & 4R). This is in contrast to MARCH5 knockdown, which promoted an increase in basal respiration and glycolysis compared with control cells (Fig 4L & 4M). Thus, these results indicate that manipulation of MARCH5 expression may reciprocally alter metabolic function, which coincides with a change in mitochondrial fusion, providing evidence that manipulating MARCH5 alters cellular respiration.

MARCH5 overexpression in vivo alters the expression of metabolic genes.

To validate the ability for MARCH5 to regulate adipocyte metabolism, we performed *in vivo* experiments in 4-week old male C57BL/6J mice (n=6/group). In these mice we injected MARCH5- or Control-recombinant adeno-associated viruses (rAAV6, $1e^{11}$vg)

subcutaneously into contralateral (opposing) inguinal fat pads of the same mouse (control on left side, MARCH5 on right side). Mice were recovered and housed for 4 weeks on a HFD to promote adipose tissue expansion (data not shown), before being culled and inguinal fat pads extracted for analysis. Gene expression analysis of the subcutaneous fat pads confirmed overexpression of *March5* (6.7±3.8 vs 7145±3095 fold change relative to control, $p<0.05$), and also demonstrated that MARCH5 overexpression in adipose tissue led to increased expression of genes associated with adipose tissue expansion and mitochondrial biogenesis including *Ppargc1a*, *Ppargc1b*, and *Pparg2* (Fig 5A & 5B). In addition, MARCH5 overexpressing fat pads exhibited increased expression of mitochondrial dynamics genes including *Mfn1*, *Mfn2* and *Dnm1l* (Fig 5C). There was no change in expression of indices of apoptosis including *Cytc*, *Fundc1* and *Bcl2* (Fig 5D). MARCH5 overexpression also induced an increase in genes involved in lipid and peroxisome metabolism including *Fasn*, *Cd36*, *Pnpla2*, *Cpt2*, *Crat* and *Crot*, and reduced expression of genes that promote lipid catabolism including *Prkab1* and *Prkab2* (AMPK subunits) (Fig 5E). The robust reductions in *Fasn* were also observed in our MARCH5 knockdown 3T3-L1 cells (Supporting Information Fig S3), consistent with *Fasn* being a potentially critical gene in the MARCH5 phenotype. Collectively, these data are consistent with the hypothesis that MARCH5 regulates mitochondrial dynamics and lipid metabolism in adipose tissue *in vivo*, similar to that observed in 3T3-L1 adipocytes.

Overall, our data demonstrate that MARCH5 expression regulates mitochondrial metabolism in adipocytes both *in vitro* and *in vivo,* and this is likely due to its role in modulating mitochondrial dynamics and substrate utilisation in the mitochondria.

Discussion

Maintaining an appropriate ability to manipulate mitochondrial dynamics and thus health, is critical for the maintenance of overall cellular health. MARCH5 is an outer mitochondrial membrane protein that has been shown to regulate several processes involved in maintaining mitochondrial dynamics including fusion, fission and apoptosis (34). Furthermore, several studies over the past 5-10 years have demonstrated an important role for mitochondrial activity to impact on adipose tissue health and function. Here, we show that MARCH5 is highly enriched in both white and brown adipose tissue, suggesting that MARCH5 is critical to adipocyte function.

Given that MARCH5 is a mitochondrial associated protein, it is reasonable to assume that it might be highly expressed in tissues that are high in mitochondria. However, our data does not support this notion, particularly with respect to the low expression observed in skeletal muscle (which is high in mitochondria), and high expression in WAT (which is low in mitochondria). Instead, our data provides strong evidence that MARCH5 is regulated by the adipogenic program, consistent with its enriched expression in adipose tissues. Indeed, we observed that MARCH5 expression in adipocytes is likely regulated by the nuclear receptor PPARγ, and that experimentally manipulating MARCH5 expression regulates mitochondrial respiration in adipocytes. This study is the first to demonstrate that MARCH5 is regulated by PPARγ during adipocyte differentiation. Importantly, suppression of PPARγ expression in hypertrophic adipocytes is observed in the setting of obesity, and this may explain the reduction in mitochondrial gene expression, including *March5*. This notion is supported by our

findings showing that *March5* expression is negatively correlated with fat mass in rodents and humans, and that *March5* is directly regulated by PPARγ as shown by ChIP-Seq analysis. It is also possible that C/EBPα plays a role in regulating the expression of *March5* due to its proximity at the *March5* promoter along with PPARγ. Adipogenic genes are known to be regulated by both C/EBPα and PPARγ during adipogenesis, and both C/EBPα and PPARγ are often found to co-exist at adipogenic gene promoters in ChIP-seq datasets. We demonstrate that loss of PPARγ is sufficient to prevent adipogenesis and *March5* expression, however we have not performed the same experiments with C/EBPα depletion, thus the precise mechanism of regulation remains to be determined in future studies.

We observed that MARCH5 expression was directly linked with mitochondrial metabolism in 3T3L1 adipocytes, since MARCH5 knockdown increased glycolysis and basal mitochondrial respiration, whilst MARCH5 overexpression decreased these parameters. Cells overexpressing MARCH5 maintained FCCP uncoupled respiration which suggests that these mitochondria were still functioning normally when stimulated with uncoupling compounds, such as FCCP. The mechanisms by which MARCH5 manipulates adipocyte metabolism are not known and require further investigation, but may involve the ability of MARCH5 to promote mitochondrial fusion. Indeed, previous reports show that MARCH5 regulates mitochondrial fusion by ubiquinating Mfn2, thereby manipulating mitochondrial morphology and altering metabolic homeostasis (3, 9, 20, 24, 33). Our studies using confocal microscopy and western blot for Mfn2 show that knock down of MARCH5 in 3T3-L1 adipocytes promotes mitochondrial fusion

compared with control cells. This is supported by similar observations in the fusion protein Mfn2 in immortalised MARCH5 KO MEFs, likely also facilitating a pro-fusion phenotype in these cells.

Previous studies have shown that mitochondrial fusion occurs as an adaptation to starvation to promote a more energy efficient mitochondrial pool, allowing energy production to be maintained in the presence of altered substrate availability (15, 36, 38, 45). As MARCH5 expression is reduced in obesity, loss of MARCH5 might be a mechanism by which the adipocyte can promote mitochondrial fusion in an attempt to alter metabolic preferences. This may suggest MARCH5 is part of a co-ordinated interplay between metabolism, mitochondrial fusion and subsequent retained capacity to generate energy.

A switch in substrate preference may also promote altered metabolic outputs, where changes in lipid metabolism or β-oxidation could lead to increased basal mitochondrial respiration, whilst maintaining other metabolic parameters such as uncoupled respiration. Consistent with this, we observed an increase in glucose uptake in cells depleted of MARCH5, which may account for the increase in glycolysis and basal mitochondrial respiration that we observe in these cells. Interestingly, when we overexpress MARCH5 *in vivo* there is an increase in the expression of key regulators of lipid metabolism, which further suggests that MARCH5 may play a role in mitochondrial substrate utilisation. Increased expression of genes involved in lipid uptake and synthesis from subcutaneous fat pads over expressing MARCH5 suggest that the alterations in lipid metabolism could be favouring the storage of excess energy.

Notably, *Crat* and *Crot* gene expression is elevated *in vivo* when March5 is overexpressed. This is curious given that *March5* is a PPARγ target gene, and that PPARγ was discovered for its role in expanding peroxisomes, thus it is possible that manipulation of MARCH5 somehow impacts on peroxisome function. *Crat* and *Crot* also play a role in the transport of very long chain fatty acids between the peroxisome, cytosol and mitochondria. Future studies should investigate whether MARCH5 directly degrades mitochondrial transporters, leading to a change not only in mitochondrial fusion, but also substrate utilisation. Such a pathway would provide an elegant mechanism for regulating mitochondrial fusion, substrate utilisation and energy output in response to changes in cellular energy requirements.

As the purpose of this study was to investigate the role of MARCH5 in adipose tissue, we also investigated whether MARCH5 expression was playing a role in browning of WAT. Although we observed increased expression of MARCH5 protein in brown adipose tissue compared to WAT in mice, we were unable to show any changes in browning related genes following MARCH overexpression either *in vitro* or *in vivo* (data not shown), suggesting that MARCH5 in this setting is not affecting browning of WAT. In the context of previously published data, our findings indicate that MARCH5 likely regulates mitochondrial morphology and dynamics in adipocytes by controlling mitochondrial fusion. Preceding studies have demonstrated that MARCH5 manipulates mitochondrial morphology by regulating the abundance of Mfn2 and Drp1, although there is some conjecture as to whether deletion of MARCH5 leads to a pro-fusion or pro-fission phenotype. Our study is the first to investigate MARCH5 in adipose cells and

tissue, and our findings suggest that loss of MARCH5 in adipocytes leads to increased mitochondrial fusion.

Overall these results demonstrate that MARCH5 expression is negatively associated with fat mass, is regulated by PPARγ, and that changes in MARCH5 expression can alter mitochondrial and cellular metabolism. These functions likely alter the utilisation of lipid, which subsequently impacts glucose metabolism. More broadly speaking, these data provide further evidence that alterations to pathways important for mitochondrial function have a significant impact on adipocyte function. However, whether these pathways can be targeted or manipulated for metabolic benefit *in vivo*, remains unanswered.

Materials and Methods

Cell Culture

3T3-L1 cells were cultured in DMEM (GIBCO #11965-084) supplemented with 10% NBCS and maintained in 5% CO_2 at 37°C. Cells were differentiated in DMEM supplemented with 10% FBS, 20nM Insulin, 50nM GW1929, 0.5mM IBMX, 1μM DEX for 48 hrs and then cultured in DMEM supplemented with 10% FBS and 20nM insulin for 10 days. WT and MITOL (MARCH5) knockout mouse embryonic fibroblasts (MEF) cells (Gift from Shigeru Yanagi, Tokyo University, Japan) were cultured in DMEM supplemented with 10% FBS and maintained in 5% CO_2 at 37°C. Primary adipocytes were isolated and cultured from inguinal fat pads as previously described (5) from floxed (fl/fl) or adipose specific PPARγ-KO (fl/fl aP2-cre) mice. Confluent pre-adipocytes were induced to differentiate in the same media as described above to induce 3T3-L1 adipocytes and imaged or harvested for protein/RNA as described below.

shRNA Knockdown and MARCH5 Expression Constructs

3T3-L1 adipocytes depleted for MARCH5 (shMARCH5) and control (luciferase - shLuc) were generated using commercially sourced lentiviral particles (Sigma MISSION particles) expressing shRNAs designed via the Broad Institutes RNAi Consortium database (TRCN0000246413 and SHC002V, respectively). Briefly, 50,000 undifferentiated 3T3-L1 cells were plated and exposed to lentiviruses (MOI = 20) in the presence of polybrene (10μg/mL) for 24 hours, before being changed in to normal growth medium (DMEM + 10% NBCS) overnight. The following day positive cells stably expressing shRNAs were selected in puromycin (4μg/mL) for 4 days, before returning cells to normal growth media prior to differentiation. Adenoviruses for human MARCH5

and GFP were generated using the VIRAPOWER kit from Invitrogen according to the manufacturer's instructions. Human MARCH5 cDNA was cloned from HEK293A cells. Adenoviruses were titred according to expression of their 3' V5-tag using an in house qPCR assay (Supporting Information Table S2), and then equivalent titres added to differentiated 3T3-L1 cells at day 7. Cells were studied on day 10.

HMDP, METSIM and Human Biopsy Studies

Microarray data generated from white adipose tissue (WAT) of mice in the Hybrid Mouse Diversity Panel was correlated with other transcripts and strain phenotypes as previously described (25). Correlations were analysed as a mid-weight bicorrelation and all data presented were significant at an FDR of 5%. METSIM data was generated by microarray analysis of adipose tissue biopsies from 770 male participants as previously described (4). Correlation analysis was performed against 23 cardio-metabolic phenotypes at an FDR of 1%. For human samples used in western blotting analysis, subcutaneous adipose tissue biopsies were obtained using standard aseptic technique and local anaesthesia (lignocaine). A 0.5-1 cm skin incision was made ~5cm lateral to the navel/umbilicus, and a Bergstrom biopsy needle passed through to obtain approximately 1-2cm^3 of subcutaneous adipose tissue under suction. All biopsies were rinsed of blood in ice-cold sterile saline, the connective tissue removed and cleaned adipose tissue was snap frozen in liquid nitrogen for subsequent storage at -80℃ until further analysis. Samples were grouped according to lean/obese and metabolic status, and blotted for indicated proteins. Pathway analysis was performed using The Database for Annotation, Visualization and Integrated Discovery (DAVID v6.8) hosted by the National Institute of Allergy and Infectious Diseases (NIAID), NIH, USA. Briefly, gene

sets were entered as a gene list in DAVID. Background adjustment was enabled against the *mus musculus* reference gene set and functional annotation clustering was performed with the classification stringency set at medium and p-value data presented as Benjamini-Hochberg corrected.

Metabolic Flux Assays

All metabolic flux analyses were performed using the Seahorse XFe96 Extracellular Flux Analyser (Agilent, Santa Clara, USA). 3T3-L1 cells were plated in a 96 well Seahorse V3-PS plate post differentiation for analyses at 1.5 x 10^4 cells per well. Cells were incubated overnight at 37°C and 5% CO_2 and prior to the assay the cells were washed with either OCR assay media (Seahorse XF base medium supplemented with 25mM glucose, 1mM glutamine and 1mM sodium pyruvate) or ECAR assay media (Seahorse XF base medium supplemented with 1mM glutamine). Cells were then equilibrated in 175µl/well of respective assay media and incubated at 37°C with no CO_2 for 30-60 minutes. The assay protocol consisted of repeat cycles of 3 minute mix, 2 minute wait and 3 minute measurement, with OCR and ECAR measured simultaneously. Basal energetics were established after four of these initial cycles followed by either mitochondrial stress test or glycolysis stress test. The mitochondrial stress test consists of sequential injections of the following compounds and 3 subsequent repeat measurements of OCR after each: The ATP synthase inhibitor oligomycin (1µM), the proton ionophore carbonyl cyanide-4-(trifluoromethoxy) phenylhydrazone (FCCP, 1µM), and the mitochondrial complex III and complex I inhibitors antimycin A/rotenone (1µM). The glycolysis stress test measures ECAR and consists of sequential injections of the following compounds after four basal

measurements: Glucose (10mM), oligomycin (1μM), and 2-deoxy-glucose (2DG, 50mM), from which glycolysis and glycolytic capacity can be determined, as ECAR is a proxy measure of glycolysis. Glycolytic capacity is the sum of the glycolytic rate and reserve glycolytic capacity. All analysis were performed with 8-23 replicates for each independent experiment. At the completion of each assay cells were lysed and protein concentration determined using the Bradford method (Bio-Rad, Sydney, Australia) according to the manufacturer's instructions.

Glucose Uptake Assay

shLuc and shMARCH5 3T3-L1 cells were grown in 12 well plates to day 7 post differentiation and glucose uptake performed as previously described (7).

Oil Red-O

shLuc and shMARCH5 3T3-L1 cells were grown in 12 well plates to day 10 post differentiation to allow for lipid loading. Cells were stained with Oil Red O as previously described (39) and imaged using an inverted Olympus IX71.

SDS-PAGE and Immunoblot

Cells were harvested and lysed in radio-immunoprecipitation assay (RIPA) buffer supplemented with protease and phosphatase inhibitors. Matched protein quantities were separated by SDS-PAGE and transferred to PVDF membranes. Membranes were blocked in 3% skim milk for 2 hours and then incubated with the appropriate primary antibody overnight at 4°C. After incubation the membranes were probed with their respective HRP-conjugate secondary antibodies (anti mouse/rabbit) in 3% skim milk for

2 hours at room temperature, then visualised with chemiluminescence (Pierce). The following primary antibodies were used: PPARγ (1:2000, Cell Signalling), Mfn2 (1:2000, Cell Signalling), Drp1 (1:2000, Cell Signalling), OXPHOS (1:2000, Mitosciences), Porin (1:2000, Mitosciences), SETDB1 (1:2000, ABCAM), Pan 14-3-3 (1:5000, Santa Cruz), MARCH5/MITOL (1:5000, gift from S. Yanagi). The Image Lab Program was used to perform densitometry analyses, where all quantification results were normalised to their respective loading control (14-3-3). Approximated molecular weights of proteins were determined from a co-resolved molecular weight standard (BioRad, #1610374).

qPCR and ChIP-Seq Analysis

RNA was isolated from cells and tissues using RNAzol reagent and isopropanol precipitation. 1µg of cDNA was generated from RNA using MMLV reverse transcriptase (Invitrogen) according to the manufacturer's instructions. qPCR was performed on 20ng cDNA using the SYBR-green method on an ABI 7500, using primer sets as outlined in Table 3. Quantification of a given gene using qPCR, was expressed by one of two ways. 1. Relative mRNA level compared with control was calculated after normalisation to a housekeeping gene *cyclophilin A* (*Ppia)* or *ribosomal protein-large-p0* (*Rplp0)* using the delta-CT method or 2. Gene expression was quantified as "normalized RNA quantity" by interpolating adjusted CT values from a $\log_{10}$ dilution curve previously generated for a given gene and primer set. Primers were designed to span exon-exon junctions and were tested for specificity using BLAST (Basic Local Alignment Search Tool; National Centre for Biotechnology Information). Amplification of a single amplicon was estimated from melt curve analysis, ensuring only a single peak with an expected temperature

dissociation profile was observed. Analysis of PPARγ (GSM340799), RXRα (GSM340805), and C/EBPα (GSM678392) occupancy in proximity to *March5* gene was completed using Integrated Genome Browser using publicly available ChIP-seq datasets deposited through NCBI of 3T3-L1 adipocytes after 6-days of differentiation (21, 29).

Confocal

Cells were grown on glass coverslips then stained with 150nM MitoTracker Deep Red (Cell Signalling) for 30 minutes. After 3 washes in 1 X PBS, cells were fixed in 4% paraformaldehyde in PBS for 30min and then washed a further 3 times in 1 X PBS. Cells were visualised on a Confocal Nikon A1r. Quantification of mitochondrial networking was performed using the Mitochondrial Network Analysis (MiNA) macro plugin tool for Fiji ImageJ. Mitochondrial network size was calculated by quantifying the average number of mitochondrial branches in three different sections of individual cells (three cells per group).

Animal experiments

All animal experiments were approved by the Alfred Medical Research and Education Precinct (AMREP) Animal Ethics committee (E/1618/2016/B). MARCH5 and control AAV6 vectors were generated by the Baker Institute AAV core as previously described (17). Four week old male C57Bl/6J mice were sourced from the AMREP Animal Centre and randomly selected for injection under isoflurane with 50µl AAV solution at $1x10^{11}$ vector genomes (vg) in PBS into contralateral inguinal regions (MARCH5 or control

vector on one of either sides). These mice were then fed a high-fat diet (43% energy from fat, #SF04-001) for 4 weeks with access to food and water *ad libitum*. Tissues from *ob/ob* mice were collected and analysed as previously described (5). All mice were housed at 22°C on a 12hr light/dark cycle.

Statistical Analysis

All animal and laboratory data were expressed as mean ± standard error of the mean (SEM). Human characteristic data from western blotting study is presented as mean ± standard deviation. All statistical analyses was performed using PRISM7 software. Groups in cell culture experiments were compared by paired students t-test. Animal studies were analysed by two-way ANOVA. Human characteristics data were analysed by two-tailed heteroscedastic t-test. A p-value of $p<0.05$ was considered statistically significant. Details for mid-weight bicorrelation analysis for HMDP and METSIM datasets can be found in their respective publications, and here: https://labs.genetics.ucla.edu/lusis/links.

Acknowledgements

Confocal imaging was supported by Monash Micro Imaging (Monash University, Australia). We thank Prof Shigeru Yanagi (Tokyo University, Japan) for donating MARCH5 (MITOL) KO MEF cells and the MITOL primary antibody. We acknowledge funding support from the Victorian State Government OIS program to Baker Heart & Diabetes Institute, and National Institutes of Health Grants HL121172 and HL28481 to AJL/MC. BGD and ACC are supported by National Heart Foundation of Australia, Future Leader Fellowships. We thank all of the study participants for their time, and for their support of our research. We also thanks all members of the MMA and LMCD laboratories at BHDI for their ongoing contributions.

Author contributions

BGD designed and conceived the study. STB and BGD performed all experiments and wrote the paper. All other authors provided reagents, data and resources. All authors read and edited the manuscript.

Conflicts of interest

The authors declare that they have no conflicts of interest.

References

1. **Burman JL, Pickles S, Wang C, Sekine S, Vargas JNS, Zhang Z, Youle AM, Nezich CL, Wu X, Hammer JA, Youle RJ**. Mitochondrial fission facilitates the selective mitophagy of protein aggregates. *J Cell Biol* 216: 3231-3247, 2017.
2. **Chen Z, Liu L, Cheng Q, Li Y, Wu H, Zhang W, Wang Y, Sehgal SA, Siraj S, Wang X, Wang J, Zhu Y, Chen Q**. Mitochondrial E3 ligase MARCH5 regulates FUNDC1 to fine-tune hypoxic mitophagy. *EMBO Rep* 18: 495-509, 2017.
3. **Cherok E, Xu S, Li S, Das S, Meltzer WA, Zalzman M, Wang C, Karbowski M**. Novel regulatory roles of Mff and Drp1 in E3 ubiquitin ligase MARCH5–dependent degradation of MiD49 and Mcl1 and control of mitochondrial dynamics. *Mol Biol Cell* 28: 396-410, 2017.
4. **Civelek M, Wu Y, Pan C, Raulerson CK, Ko A, He A, Tilford C, Saleem NK, Stancakova A, Scott LJ, Fuchsberger C, Stringham HM, Jackson AU, Narisu N, Chines PS, Small KS, Kuusisto J, Parks BW, Pajukanta P, Kirchgessner T, Collins FS, Gargalovic PS, Boehnke M, Laakso M, Mohlke KL, Lusis AJ**. Genetic Regulation of Adipose Gene Expression and Cardio-Metabolic Traits. *Am J Hum Genet* 100: 428-443, 2017.
5. **Drew BG, Hamidi H, Zhou Z, Villanueva CJ, Krum SA, Calkin AC, Parks BW, Ribas V, Kalajian NY, Phun J, Daraei P, Christofk HR, Hewitt SC, Korach KS, Tontonoz P, Lusis AJ, Slamon DJ, Hurvitz SA, Hevener AL**. Estrogen receptor (ER)alpha-regulated lipocalin 2 expression in adipose tissue links obesity with breast cancer progression. *J Biol Chem* 290: 5566-81, 2015.
6. **Hegarty BD, Furler SM, Oakes ND, Kraegen EW, Cooney GJ**. Peroxisome proliferator-activated receptor (PPAR) activation induces tissue-specific effects on fatty acid uptake and metabolism in vivo—a study using the novel PPARα/γ agonist tesaglitazar. *Endocrinology* 145: 3158-3164, 2004.
7. **Henstridge DC, Bruce CR, Drew BG, Tory K, Kolonics A, Estevez E, Chung J, Watson N, Gardner T, Lee-Young RS, Connor T, Watt MJ, Carpenter K, Hargreaves M, McGee SL, Hevener AL, Febbraio MA**. Activating HSP72 in rodent skeletal muscle increases mitochondrial number and oxidative capacity and decreases insulin resistance. *Diabetes* 63: 1881-94, 2014.
8. **Jian F, Chen D, Chen L, Yan C, Lu B, Zhu Y, Chen S, Shi A, Chan DC, Song Z**. Sam50 Regulates PINK1-Parkin-Mediated Mitophagy by Controlling PINK1 Stability and Mitochondrial Morphology. *Cell Rep* 23: 2989-3005, 2018.
9. **Karbowski M, Neutzner A, Youle RJ**. The mitochondrial E3 ubiquitin ligase MARCH5 is required for Drp1 dependent mitochondrial division. *J Cell Biol* 178: 71-84, 2007.
10. **Kim KY, Stevens MV, Akter MH, Rusk SE, Huang RJ, Cohen A, Noguchi A, Springer D, Bocharov AV, Eggerman TL, Suen DF, Youle RJ, Amar M, Remaley AT, Sack MN**. Parkin is a lipid-responsive regulator of fat uptake in mice and mutant human cells. *J Clin Invest* 121: 3701-12, 2011.
11. **Kiriyama Y, Nochi H**. Intra-and intercellular quality control mechanisms of mitochondria. *Cells* 7: 1, 2017.
12. **Kusminski CM, Holland WL, Sun K, Park J, Spurgin SB, Lin Y, Askew GR, Simcox JA, McClain DA, Li C, Scherer PE**. MitoNEET, a key regulator of mitochondrial function and lipid homeostasis. *Nat Med* 18: 1539-1549, 2012.

13. **Lee JE, Westrate LM, Wu H, Page C, Voeltz GK**. Multiple dynamin family members collaborate to drive mitochondrial division. *Nature* 540: 139, 2016.
14. **Lefterova MI, Zhang Y, Steger DJ, Schupp M, Schug J, Cristancho A, Feng D, Zhuo D, Stoeckert CJ, Jr., Liu XS, Lazar MA**. PPARgamma and C/EBP factors orchestrate adipocyte biology via adjacent binding on a genome-wide scale. *Genes Dev* 22: 2941-52, 2008.
15. **Liesa M, Shirihai OS**. Mitochondrial dynamics in the regulation of nutrient utilization and energy expenditure. *Cell Metab* 17: 491-506, 2013.
16. **Madsen MS, Siersbæk R, Boergesen M, Nielsen R, Mandrup S**. Peroxisome proliferator-activated receptor γ and C/EBPα synergistically activate key metabolic adipocyte genes by assisted loading. *Mol Cell Biol* 34: 939-954, 2014.
17. **Marshall JPS, Estevez E, Kammoun HL, King EJ, Bruce CR, Drew BG, Qian H, Iliades P, Gregorevic P, Febbraio MA, Henstridge DC**. Skeletal muscle-specific overexpression of heat shock protein 72 improves skeletal muscle insulin-stimulated glucose uptake but does not alter whole body metabolism. *Diabetes Obes Metab* 20: 1928-1936, 2018.
18. **Marycz K, Kornicka K, Szlapka-Kosarzewska J, Weiss C**. Excessive endoplasmic reticulum stress correlates with impaired mitochondrial dynamics, mitophagy and apoptosis, in liver and adipose tissue, but not in muscles in EMS horses. *Int J Mol Sci* 19: 165, 2018.
19. **Mitra K**. Mitochondrial fission-fusion as an emerging key regulator of cell proliferation and differentiation. *Bioessays* 35: 955-964, 2013.
20. **Nakamura N, Kimura Y, Tokuda M, Honda S, Hirose S**. MARCH-V is a novel mitofusin 2- and Drp1-binding protein able to change mitochondrial morphology. *EMBO Rep* 7: 1019-22, 2006.
21. **Nielsen R, Pedersen TA, Hagenbeek D, Moulos P, Siersbaek R, Megens E, Denissov S, Borgesen M, Francoijs KJ, Mandrup S, Stunnenberg HG**. Genome-wide profiling of PPARgamma:RXR and RNA polymerase II occupancy reveals temporal activation of distinct metabolic pathways and changes in RXR dimer composition during adipogenesis. *Genes Dev* 22: 2953-67, 2008.
22. **Nolan JJ, Ludvik B, Beerdsen P, Joyce M, Olefsky J**. Improvement in glucose tolerance and insulin resistance in obese subjects treated with troglitazone. *N Engl J Med* 331: 1188-1193, 1994.
23. **Osellame LD, Blacker TS, Duchen MR**. Cellular and molecular mechanisms of mitochondrial function. *Best Pract Res Clin Endocrinol Metab* 26: 711-23, 2012.
24. **Park Y-Y, Lee S, Karbowski M, Neutzner A, Youle RJ, Cho H**. Loss of MARCH5 mitochondrial E3 ubiquitin ligase induces cellular senescence through dynamin-related protein 1 and mitofusin 1. *J Cell Sci* 123: 619-626, 2010.
25. **Parks BW, Nam E, Org E, Kostem E, Norheim F, Hui ST, Pan C, Civelek M, Rau CD, Bennett BJ, Mehrabian M, Ursell LK, He A, Castellani LW, Zinker B, Kirby M, Drake TA, Drevon CA, Knight R, Gargalovic P, Kirchgessner T, Eskin E, Lusis AJ**. Genetic control of obesity and gut microbiota composition in response to high-fat, high-sucrose diet in mice. *Cell Metab* 17: 141-52, 2013.
26. **Parks BW, Sallam T, Mehrabian M, Psychogios N, Hui ST, Norheim F, Castellani LW, Rau CD, Pan C, Phun J, Zhou Z, Yang WP, Neuhaus I, Gargalovic PS, Kirchgessner TG, Graham M, Lee R, Tontonoz P, Gerszten**

RE, Hevener AL, Lusis AJ. Genetic architecture of insulin resistance in the mouse. *Cell Metab* 21: 334-347, 2015.

27. **Pernas L, Scorrano L**. Mito-morphosis: mitochondrial fusion, fission, and cristae remodeling as key mediators of cellular function. *Annu Rev Physiol* 78: 505-531, 2016.
28. **Samji T, Hong S, Means RE**. The Membrane Associated RING-CH Proteins: A Family of E3 Ligases with Diverse Roles through the Cell. *Int Sch Res Notices* 2014: 637295, 2014.
29. **Schmidt SF, Jorgensen M, Chen Y, Nielsen R, Sandelin A, Mandrup S**. Cross species comparison of C/EBPalpha and PPARgamma profiles in mouse and human adipocytes reveals interdependent retention of binding sites. *BMC Genomics* 12: 152, 2011.
30. **Sebastián D, Zorzano A**. Mitochondrial dynamics and metabolic homeostasis. *Current Opinion in Physiology* 3: 34-40, 2018.
31. **Seldin MM, Koplev S, Rajbhandari P, Vergnes L, Rosenberg GM, Meng Y, Pan C, Phuong TMN, Gharakhanian R, Che N, Makinen S, Shih DM, Civelek M, Parks BW, Kim ED, Norheim F, Chella Krishnan K, Hasin-Brumshtein Y, Mehrabian M, Laakso M, Drevon CA, Koistinen HA, Tontonoz P, Reue K, Cantor RM, Bjorkegren JLM, Lusis AJ**. A Strategy for Discovery of Endocrine Interactions with Application to Whole-Body Metabolism. *Cell Metab* 27: 1138-1155.e6, 2018.
32. **Singh R, Xiang Y, Wang Y, Baikati K, Cuervo AM, Luu YK, Tang Y, Pessin JE, Schwartz GJ, Czaja MJ**. Autophagy regulates adipose mass and differentiation in mice. *J Clin Invest* 119: 3329-39, 2009.
33. **Sugiura A, Nagashima S, Tokuyama T, Amo T, Matsuki Y, Ishido S, Kudo Y, McBride HM, Fukuda T, Matsushita N, Inatome R, Yanagi S**. MITOL regulates endoplasmic reticulum-mitochondria contacts via Mitofusin2. *Mol Cell* 51: 20-34, 2013.
34. **Sugiura A, Yonashiro R, Fukuda T, Matsushita N, Nagashima S, Inatome R, Yanagi S**. A mitochondrial ubiquitin ligase MITOL controls cell toxicity of polyglutamine-expanded protein. *Mitochondrion* 11: 139-146, 2011.
35. **Tontonoz P, Hu E, Spiegelman BM**. Stimulation of adipogenesis in fibroblasts by PPARγ2, a lipid-activated transcription factor. *Cell* 79: 1147-1156, 1994.
36. **Wai T, Langer T**. Mitochondrial dynamics and metabolic regulation. *Trends Endocrinol Metab* 27: 105-117, 2016.
37. **Wang J, Aung LH, Prabhakar BS, Li P**. The mitochondrial ubiquitin ligase plays an anti-apoptotic role in cardiomyocytes by regulating mitochondrial fission. *J Cell Mol Med* 20: 2278-2288, 2016.
38. **Weir HJ, Yao P, Huynh FK, Escoubas CC, Goncalves RL, Burkewitz K, Laboy R, Hirschey MD, Mair WB**. Dietary restriction and AMPK increase lifespan via mitochondrial network and peroxisome remodeling. *Cell Metab* 26: 884-896. e5, 2017.
39. **Wend K, Wend P, Drew BG, Hevener AL, Miranda-Carboni GA, Krum SA**. ERα regulates lipid metabolism in bone through ATGL and perilipin. *J Cell Biochem* 114: 1306-1314, 2013.
40. **Wilson-Fritch L, Burkart A, Bell G, Mendelson K, Leszyk J, Nicoloro S, Czech M, Corvera S**. Mitochondrial biogenesis and remodeling during

adipogenesis and in response to the insulin sensitizer rosiglitazone. *Mol Cell Biol* 23: 1085-1094, 2003.

41. **Wilson-Fritch L, Nicoloro S, Lazar MA, Chui PC, Leszyk J, Straubhaar J, Czech MP, Corvera S**. Mitochondrial remodeling in adipose tissue associated with obesity and treatment with rosiglitazone. *J Clin Invest* 114: 1281, 2004.
42. **Yonashiro R, Ishido S, Kyo S, Fukuda T, Goto E, Matsuki Y, Ohmura-Hoshino M, Sada K, Hotta H, Yamamura H, Inatome R, Yanagi S**. A novel mitochondrial ubiquitin ligase plays a critical role in mitochondrial dynamics. *EMBO J* 25: 3618-26, 2006.
43. **Yoo YS, Park YY, Kim JH, Cho H, Kim SH, Lee HS, Kim TH, Sun Kim Y, Lee Y, Kim CJ, Jung JU, Lee JS, Cho H**. The mitochondrial ubiquitin ligase MARCH5 resolves MAVS aggregates during antiviral signalling. *Nat Commun* 6: 7910, 2015.
44. **Yu M, Huang Y, Deorukhkar A, Fujimoto T, Govindaraju S, Molkentine J, Lin D, Kang Ya, Koay E, Fleming J, Gupta S, Maitra A, Taniguchi C**. Mitochondrial Fusion Suppresses Pancreatic Cancer Growth via Reduced Oxidative Metabolism. *bioRxiv* doi:10.1101/279745: 2018.
45. **Zafaranieh S, Choobineh S, Soori R**. The effect of 12 weeks of aerobic exercise on mitochondrial dynamics in cardiac myocytes of type 2 diabetic rats. *Sport Sciences for Health* 14: 305-312, 2018.
46. **Zemirli N, Morel E, Molino D**. Mitochondrial Dynamics in Basal and Stressful Conditions. *Int J Mol Sci* 19: 564, 2018.
47. **Zhang Y, Goldman S, Baerga R, Zhao Y, Komatsu M, Jin S**. Adipose-specific deletion of autophagy-related gene 7 (atg7) in mice reveals a role in adipogenesis. *Proc Natl Acad Sci U S A* 106: 19860-5, 2009.

Table 1. Correlation (mid-weight bicor) analysis of other mitochondrial transcripts (grey boxes) negatively correlated with fat mass in HMDP (mouse) and METSIM (human) databases. White boxes confirm a similar negative correlation with PPAR-gamma expression whilst an expected highly positive correlation was observed with leptin expression (dark grey boxes).

MOUSE			HUMAN		
Gene	**r-value**	**p-value**	**Gene**	**r-value**	**p-value**
Dnm1L	-0.323	1.42E-03	***DNM1L***	no human probe	
Mff	-0.49	1.01E-05	***MFF***	-0.204	4.01E-03
Opa1	-0.269	8.50E-03	***OPA1***	-0.217	2.13E-03
Rhot1	-0.353	4.52E-04	***RHOT1***	-0.428	3.07E-10
Mfn1	-0.501	2.36E-07	***MFN1***	-0.203	4.05E-03
Pparg	-0.309	2.32E-03	***PPARG***	-0.453	2.04E-11
Lep	0.708	1.07E-15	***LEP***	0.383	2.51E-08

Table 2. All transcripts that correlated with PPARγ at a bicor of r>0.5 that were analysed for pathway enrichment in Figure 2B (duplicates appear as a results of multiple probes for given transcripts)

Gene Symbol	Gene Name	R value
March5	membrane-associated ring finger (C3HC4) 5	+0.742
Pex13	peroxisomal biogenesis factor 13	+0.693
Osbpl11	oxysterol binding protein-like 11	+0.684
Ophn1	oligophrenin 1	+0.679
Cdadc1	cytidine and dCMP deaminase domain containing 1	+0.672
Klb	klotho beta	+0.672
Osbpl11	oxysterol binding protein-like 11	+0.67
Adhfe1	alcohol dehydrogenase, iron containing, 1	+0.664
Mrps31	mitochondrial ribosomal protein S31	+0.647
Sh2b2	SH2B adaptor protein 2	+0.646
BC054059	cDNA sequence BC054059	+0.646
Hibadh	3-hydroxyisobutyrate dehydrogenase	+0.643
4932441K18Rik	RIKEN cDNA 4932441K18 gene	+0.642
Adhfe1	alcohol dehydrogenase, iron containing, 1	+0.642
Slc1a3	solute carrier family 1 (glial high affinity glutamate transporter), member 3	+0.636
Slc1a3	solute carrier family 1 (glial high affinity glutamate transporter), member 3	+0.63
Kif13a	kinesin family member 13A	+0.629
Ypel5	yippee-like 5 (Drosophila)	+0.628
Tbc1d20	TBC1 domain family, member 20	+0.625
Rdh14	retinol dehydrogenase 14 (all-trans and 9-cis)	+0.625
Ptprm	protein tyrosine phosphatase, receptor type, M	+0.622
Lipe	lipase, hormone sensitive	+0.619
Trit1	tRNA isopentenyltransferase 1	+0.614
Pex3	peroxisomal biogenesis factor 3	+0.612
Acsl1	acyl-CoA synthetase long-chain family member 1	+0.611
Ankrd57	ankyrin repeat domain 57	+0.606
Cebpg	CCAAT/enhancer binding protein (C/EBP), gamma	+0.606
Ormdl3	ORM1-like 3 (S. cerevisiae)	+0.604
Abhd5	abhydrolase domain containing 5	+0.604
B3galt2	UDP-Gal:betaGlcNAc beta 1,3-galactosyltransferase, polypeptide 2	+0.603
Ppp2r1b	protein phosphatase 2 (formerly 2A), regulatory subunit A (PR 65), beta isoform	+0.602
Slc25a46	solute carrier family 25, member 46	+0.602
Slc1a3	solute carrier family 1 (glial high affinity glutamate transporter), member 3	+0.601
Acsl1	acyl-CoA synthetase long-chain family member 1	+0.6

Hibadh	3-hydroxyisobutyrate dehydrogenase	+0.6
Acacb	acetyl-Coenzyme A carboxylase beta	+0.6
Dpm1	dolichol-phosphate (beta-D) mannosyltransferase 1	+0.598
Dtnbp1	dystrobrevin binding protein 1	+0.598
Cdadc1	cytidine and dCMP deaminase domain containing 1	+0.597
Pnpla2	patatin-like phospholipase domain containing 2	+0.597
Gphn	gephyrin	+0.594
Ppm1b	protein phosphatase 1B, magnesium dependent, beta isoform	+0.592
B3galt2	UDP-Gal:betaGlcNAc beta 1,3-galactosyltransferase, polypeptide 2	+0.591
Gpam	glycerol-3-phosphate acyltransferase, mitochondrial	+0.591
Nedd4	neural precursor cell expressed, developmentally down-regulated 4	+0.59
Gpam	glycerol-3-phosphate acyltransferase, mitochondrial	+0.589
Tbc1d20	TBC1 domain family, member 20	+0.589
Bag4	BCL2-associated athanogene 4	+0.589
Bag4	BCL2-associated athanogene 4	+0.588
Ces3	carboxylesterase 3	+0.588
Bnip3l	BCL2/adenovirus E1B interacting protein 3-like	+0.587
Nr1h3	nuclear receptor subfamily 1, group H, member 3	+0.586
Cfd	complement factor D (adipsin)	+0.586
1110002N22Rik	RIKEN cDNA 1110002N22 gene	+0.584
Sfxn1	sideroflexin 1	+0.583
Acsl1	acyl-CoA synthetase long-chain family member 1	+0.583
Ifrd1	interferon-related developmental regulator 1	+0.583
Parp6	poly (ADP-ribose) polymerase family, member 6	+0.581
Eltd1	EGF, latrophilin seven transmembrane domain containing 1	+0.579
Gys1	glycogen synthase 1, muscle	+0.577
Echs1	enoyl Coenzyme A hydratase, short chain, 1, mitochondrial	+0.576
5730469M10Rik	RIKEN cDNA 5730469M10 gene	+0.576
Baz1b	bromodomain adjacent to zinc finger domain, 1B	+0.574
Lamb1-1	laminin B1 subunit 1	+0.573
Fbxw2	F-box and WD-40 domain protein 2	+0.573
Cat	catalase	+0.572
Crat	carnitine acetyltransferase	+0.571
1300001I01Rik	RIKEN cDNA 1300001I01 gene	+0.57
Etv3	ets variant gene 3	+0.568
Hspa9	heat shock protein 9	+0.568
Atl2	atlastin GTPase 2	+0.567
Tshr	thyroid stimulating hormone receptor	+0.566
Acvr1c	activin A receptor, type IC	+0.566
Csad	cysteine sulfinic acid decarboxylase	+0.565

Dnase2a	deoxyribonuclease II alpha	+0.564
Aldh6a1	aldehyde dehydrogenase family 6, subfamily A1	+0.564
Gphn	gephyrin	+0.563
Nup54	nucleoporin 54	+0.561
Dgat1	diacylglycerol O-acyltransferase 1	+0.56
Acot4	acyl-CoA thioesterase 4	+0.559
Orc3l	origin recognition complex, subunit 3-like (S. cerevisiae)	+0.559
Sec24b	Sec24 related gene family, member B (S. cerevisiae)	+0.558
Fabp4	fatty acid binding protein 4, adipocyte	+0.555
Zkscan3	zinc finger with KRAB and SCAN domains 3	+0.555
Sox6	SRY-box containing gene 6	+0.555
Acsm3	acyl-CoA synthetase medium-chain family member 3	+0.553
Ncoa4	nuclear receptor coactivator 4	+0.553
Pus10	pseudouridylate synthase 10	+0.553
Gpcpd1	glycerophosphocholine phosphodiesterase GDE1 homolog (S. cerevisiae)	+0.553
Dbt	dihydrolipoamide branched chain transacylase E2	+0.552
Cul2	cullin 2	+0.55
N4bp2l1	NEDD4 binding protein 2-like 1	+0.55
Fbxw2	F-box and WD-40 domain protein 2	+0.548
Srfbp1	serum response factor binding protein 1	+0.548
Ephx2	epoxide hydrolase 2, cytoplasmic	+0.548
Etfa	electron transferring flavoprotein, alpha polypeptide	+0.547
Hibch	3-hydroxyisobutyryl-Coenzyme A hydrolase	+0.547
Sgpl1	sphingosine phosphate lyase 1	+0.546
Pgrmc2	progesterone receptor membrane component 2	+0.543
St7l	suppression of tumorigenicity 7-like	+0.543
Ccnl2	cyclin L2	+0.542
Slc9a3r2	solute carrier family 9 (sodium/hydrogen exchanger), member 3 regulator 2	+0.542
Pcmtd1	protein-L-isoaspartate (D-aspartate) O-methyltransferase domain containing 1	+0.542
Ngly1	N-glycanase 1	+0.541
Phyh	phytanoyl-CoA hydroxylase	+0.541
Psmc1	protease (prosome, macropain) 26S subunit, ATPase 1	+0.541
Tmed5	transmembrane emp24 protein transport domain containing 5	+0.541
Sdha	succinate dehydrogenase complex, subunit A, flavoprotein (Fp)	+0.54
Cox4nb	COX4 neighbor	+0.54
Abhd15	abhydrolase domain containing 15	+0.54
Vegfa	vascular endothelial growth factor A	+0.54
Unknown	Unannotated gene	+0.54
Ranbp9	RAN binding protein 9	+0.54
AU018778	expressed sequence AU018778	+0.539

Unknown	Unannotated gene	+0.538
Pitpnb	phosphatidylinositol transfer protein, beta	+0.538
Pum1	pumilio 1 (Drosophila)	+0.538
Sfxn1	sideroflexin 1	+0.537
Abhd5	abhydrolase domain containing 5	+0.537
Mccc2	methylcrotonoyl-Coenzyme A carboxylase 2 (beta)	+0.537
Ncoa4	nuclear receptor coactivator 4	+0.536
Hmgcl	3-hydroxy-3-methylglutaryl-Coenzyme A lyase	+0.536
Lpl	lipoprotein lipase	+0.535
Eif2b1	eukaryotic translation initiation factor 2B, subunit 1 (alpha)	+0.535
Cdadc1	cytidine and dCMP deaminase domain containing 1	+0.534
Cirh1a	cirrhosis, autosomal recessive 1A (human)	+0.533
Irs1	insulin receptor substrate 1	+0.533
Eif3j	eukaryotic translation initiation factor 3, subunit J	+0.533
Sh2b2	SH2B adaptor protein 2	+0.532
Dpp8	dipeptidylpeptidase 8	+0.531
Ophn1	oligophrenin 1	+0.53
Mkks	McKusick-Kaufman syndrome protein	+0.53
Eltd1	EGF, latrophilin seven transmembrane domain containing 1	+0.529
Mgst1	microsomal glutathione S-transferase 1	+0.529
Isca1	iron-sulfur cluster assembly 1 homolog (S. cerevisiae)	+0.529
Pnpla8	patatin-like phospholipase domain containing 8	+0.529
C80913	expressed sequence C80913	+0.527
Ube4b	ubiquitination factor E4B, UFD2 homolog (S. cerevisiae)	+0.527
Sec24b	Sec24 related gene family, member B (S. cerevisiae)	+0.526
Kif1b	kinesin family member 1B	+0.526
Pcmtd1	protein-L-isoaspartate (D-aspartate) O-methyltransferase domain containing 1	+0.526
Sgpl1	sphingosine phosphate lyase 1	+0.525
Timp3	tissue inhibitor of metalloproteinase 3	+0.525
Pecam1	platelet/endothelial cell adhesion molecule 1	+0.525
Pccb	propionyl Coenzyme A carboxylase, beta polypeptide	+0.524
Rad21	RAD21 homolog (S. pombe)	+0.524
Pex14	peroxisomal biogenesis factor 14	+0.523
Atl2	atlastin GTPase 2	+0.523
Bnip3	BCL2/adenovirus E1B interacting protein 3	+0.522
Gosr1	golgi SNAP receptor complex member 1	+0.522
Chpt1	choline phosphotransferase 1	+0.521
Usp47	ubiquitin specific peptidase 47	+0.521
1500003O03Rik	RIKEN cDNA 1500003O03 gene	+0.52
Atp1a2	ATPase, Na+/K+ transporting, alpha 2 polypeptide	+0.52
Mapk6	mitogen-activated protein kinase 6	+0.52

Ppm1a	protein phosphatase 1A, magnesium dependent, alpha isoform	+0.519
Aldh2	aldehyde dehydrogenase 2, mitochondrial	+0.519
Sfrs1	splicing factor, arginine/serine-rich 1 (ASF/SF2)	+0.519
Ywhab	tyrosine 3-monooxygenase/tryptophan 5-monooxygenase activation protein, beta polypeptide	+0.519
Pex3	peroxisomal biogenesis factor 3	+0.518
Tomm70a	translocase of outer mitochondrial membrane 70 homolog A (yeast)	+0.518
Sdpr	serum deprivation response	+0.516
Slc27a1	solute carrier family 27 (fatty acid transporter), member 1	+0.516
Acox1	acyl-Coenzyme A oxidase 1, palmitoyl	+0.516
Zkscan3	zinc finger with KRAB and SCAN domains 3	+0.515
Baz1b	bromodomain adjacent to zinc finger domain, 1B	+0.514
Ppargc1b	peroxisome proliferative activated receptor, gamma, coactivator 1 beta	+0.514
Rcl1	RNA terminal phosphate cyclase-like 1	+0.514
Gys1	glycogen synthase 1, muscle	+0.514
Etv3	ets variant gene 3	+0.514
Phax	phosphorylated adaptor for RNA export	+0.513
Psmd4	proteasome (prosome, macropain) 26S subunit, non-ATPase, 4	+0.512
Seh1l	SEH1-like (S. cerevisiae	+0.512
Timp3	tissue inhibitor of metalloproteinase 3	+0.512
Pabpc4	poly(A) binding protein, cytoplasmic 4	+0.511
Crbn	cereblon	+0.51
Cebpz	CCAAT/enhancer binding protein zeta	+0.51
Pim3	proviral integration site 3	+0.509
Timm50	translocase of inner mitochondrial membrane 50 homolog (yeast)	+0.509
Btf3l4	basic transcription factor 3-like 4	+0.509
Aacs	acetoacetyl-CoA synthetase	+0.509
Tfdp1	transcription factor Dp 1	+0.509
Mtch2	mitochondrial carrier homolog 2 (C. elegans)	+0.508
Bscl2	Bernardinelli-Seip congenital lipodystrophy 2 homolog (human)	+0.507
Bscl2	Bernardinelli-Seip congenital lipodystrophy 2 homolog (human)	+0.506
Bckdha	branched chain ketoacid dehydrogenase E1, alpha polypeptide	+0.506
Pex5	peroxisomal biogenesis factor 5	+0.506
Aacs	acetoacetyl-CoA synthetase	+0.505
Mknk2	MAP kinase-interacting serine/threonine kinase 2	+0.505
Ddx27	DEAD (Asp-Glu-Ala-Asp) box polypeptide 27	+0.505
Rsl1d1	ribosomal L1 domain containing 1	+0.505
Ubqln1	ubiquilin 1	+0.504
Entpd5	ectonucleoside triphosphate diphosphohydrolase 5	+0.504
Sh3glb1	SH3-domain GRB2-like B1 (endophilin)	+0.504
Psmd12	proteasome (prosome, macropain) 26S subunit, non-ATPase, 12	+0.503

Snrnp48	small nuclear ribonucleoprotein 48 (U11/U12)	+0.503
Cept1	choline/ethanolaminephosphotransferase 1	+0.503
Mapk6	mitogen-activated protein kinase 6	+0.502
Unknown	Unannotated gene	+0.502
Taf1d	TATA box binding protein (Tbp)-associated factor, RNA polymerase I, D	+0.501
Stag2	stromal antigen 2	+0.501
Hspa9	heat shock protein 9	+0.501
Eri2	exoribonuclease 2	+0.501
S100a1	S100 calcium binding protein A1	+0.501
Kif1b	kinesin family member 1B	+0.501
Rabggtb	RAB geranylgeranyl transferase, b subunit	+0.501
Pak2	p21 protein (Cdc42/Rac)-activated kinase 2	+0.5
Grb10	growth factor receptor bound protein 10	+0.5
Rasip1	Ras interacting protein 1	+0.5
Mrpl50	mitochondrial ribosomal protein L50	+0.5
Nbn	nibrin	+0.5

774

775

Table 3. Primers for qPCR. (m = mouse, h = human, p = plasmid/synthetic).

Gene name	Primer sequence Forward (5'-3')	Primer sequence Reverse (5'-3')
mMfn2	ATTGATCACGGTGCTCTTCC	GTCCTGGACGTCAAAGGGTA
mDnm1L	TGCCTCAGATCGTCGTAGTG	CGTGGACTAGCTGCAGAATG
mPparg	GTGCCAGTTTCGATCCGTAGA	GGCCAGCATCGTGTAGATGA
mPparg2	GTTTTATGCTGTTATGGGTG	GTAATTTCTTGTGAAGTGCTCATAG
mMarch5	TTGGACAGCCGTGACTTATG	AGGGTCAGCTCGCTCCAT
hMARCH5	CAAAAGCCTGTCCATTTGC	CCAGACCTTCTTTATGACCTACAAC
mPgc1a	TGAGGACCGCTAGCAAGTTT	TGAAGTGGTGTAGCGACCAA
mPgc1b	CTGAGTCAAAGTCACTGGCG	GCTCTCGTCCTTCTTCCTCA
mCebpa	TGGACAAGAACAGCAACGAG	GTCACTGGTCAACTCCAGCA
mCd36	TTGTACCTATACTGTGGCTAAATGAGA	CTTGTGTTTTGAACATTTCTGCTT
mLdlr	AGGCTGTGGGCTCCATAGG	TGCGGTCCAGGGTCATCT
mSlc27a1	GACAAGCTGGATCAGGCAAG	GAGGCCACAGAGGCTGTTC
mCptc1c	GTGGACAAGCACCAGGCTCT	TGGACCTGGGTCAGGAAGGG
mCpt2	ACAGTGTGGGCGAGCTTCAG	GGCTGCTGCCAGATACCGTAG
mDgat2	CACTCCAGTGGGTTCCGTGT	TTTGGCCTTGACCCTTCGCT
mBcl2	AGGGTCTTCAGAGACAGCCA	AGTACCTGAACCGGCATCTG
mCytc	CAGCTTCCATTGCGGACAC	CGCTGACAGCATCACCTTTC
mFundc1	ATTGTAATGGGTGGCGTGAC	CATAGCCACTGTGACTGGCA
mFasn	TGCTCCCAGCTGCAGGC	GCCCGGTAGCTCTGGGTGTA
mPnpla2	GAAATTGGGTGACCATCTGC	TGGGTAGGGCCTCACTGTAG
mCrat	AACTGGCTGTCCGAGTGGTG	TGGCAGCAAACCGAAGCTGA
mCrot	GACTTCATGGACGCCCTGGT	ACCTGACGGCCTCCACTGTA
mGfp	CAGGAGCGCACCATCTTCTT	CTTGTGCCCCAGGATGTTG
mCidea	TGCTCTTCTGTATCGCCCAGT	GCCGTGTTAAGGAATCTGCTG
mPrkaca	CCCACCCTTCTTCGCTGACC	GTTCCGCAGCAGGTCCTTCA
mPrkab1	CGGGCATCTCTTGTGACCCA	GCACTGAGCACCATCACTCCA
mPrkab2	TCTCCTTGTACGCCGAACAGC	CCCGCTCGCTGGTAGTGTTT
mFabp4	GGTCGACTTTCCATCCCACTT	TTCGATGAAATCACCGCAGA
mLpl	TTTGTGAAATGCCATGACAAG	CAGATGCTTTCTTCTCTTGTTTGT
mLipe	GCGCTGGAGGAGTGTTTTT	CCGCTCTCCAGTTGAACC
pAD-V5	CCTAACCCTCTCCTCGGTCT	TCTGTCTTTTTATTGCCGTCAT
mPpia	AGCCAAATCCTTTCTCTCCAG	CACCGTGTTCTTCGACATCA
mRplp0	ACCCTGAAGTGCTCGACATC	ATTGATGATGGAGTGTGGCA

Figure Legends

Figure1: *March5* expression is negatively correlated with obesity phenotypes in rodents and humans. (A) Heat map depicts correlations between *March5* mRNA expression and adiposity/metabolism traits from mouse strains of the HMDP (n=101 strains). (B) Dot plot and linear regression of white adipose tissue (WAT) *March5* mRNA expression with fat mass (grams - g) as determined by EchoMRI in 101 strains of the HMDP (each dot represents an individual strain). (C) Bar graph for *March5* gene expression in WAT from wild-type (WT) and *ob/ob*, normalised to *Cyclophilin A* (*Ppia*) gene expression. (D) Dot plot and linear regression of WAT *March5* mRNA expression with fat mass (kilograms – kg) in 770 male individuals from the METSIM study (each dot represents one individual). (E) Western blots for MARCH5, PPARγ and 14-3-3 (loading control) from subcutaneous WAT biopsies taken from lean, normal glucose tolerant (NGT) individuals versus obese, impaired fasting blood glucose (iFBG) male individuals. (F & G) Densitometric quantification of MARCH5 and PPARγ protein levels normalised to 14-3-3. All data are presented as mean±SEM, *p<0.05 from WT or lean samples. MRI – Magnetic Resonance Imaging; FFA - Free Fatty Acid; Chol - Cholesterol; TG - Triglycerides; FFP- Femoral (subcutaneous) Fat Pad; GFP - Gonadal Fat Pad; MFP - Mesenteric Fat Pad; RFP – Retroperitoneal Fat Pad; % - Tissue weight as a percentage of total body weight.

Figure 2: MARCH5 is highly expressed in adipose tissue and is regulated by PPARγ.

(A) Dot plot depicting genes significantly (FDR 5%) positively correlated (bicor r>0.4) with PPARγ expression in WAT of HMDP strains; red dots = previously validated PPARγ target genes, blue dot = *March5*. (B) Pathway enrichment analysis of genes correlated (bicor r>0.5) with PPARγ in WAT from strains of the HMDP (C) Western blots for MARCH5 and 14-3-3 (loading control) in WAT and BAT from C57BL/6J mice. (D) Bar graph of gene expression analysis for *March5* mRNA in various tissues of C57BL/6J mice (n=5, mean±SEM). (E) ChIP-seq analysis of PPARγ, RXRα and C/EBPα at the *March5* locus in 3T3-L1 adipocytes (F) Photomicrographs of pre-differentiated (Pre-Diff) and differentiated (day 7 – Diff) primary adipocytes isolated from WT (PPARγ floxed) and PPARγ-KO (PPARγ floxed + aP2-cre) C57BL/6J mice and subsequent (G) bar graph of gene expression analysis for *March5* normalised to *Cyclophilin A* (*Ppia*) in those cells. Values represent means ±SEM, * p<0.05 from non-diff WT, # p<0.05 from WT non-diff. WAT = white adipose tissue, BAT = brown adipose tissue, Hrt = heart, Quad = quadriceps, Sol = soleus, Liv = liver.

Figure 3: PPARγ and mitochondrial protein expression, including MARCH5 are increased during adipocyte differentiation.

(A) Western blot and densitometric quantification of MARCH5 and Mitofusin2 (Mfn2) from WT and MARCH5-KO MEFs, adjusted for loading control (14-3-3). (B & C) Western blot and densitometry analyses of adipogenic and mitochondrial proteins from pre-differentiated through day 10 post-differentiated 3T3-L1 adipocytes. All data are presented as mean±SEM, *p<0.05. Drp1 = dynamin related protein 1, Complex V =

824 Complex V of the mitochondrial electron transport chain, MEF = mouse embryonic
825 fibroblast, DMI = dexamethasone/methyl-3-isobutylxanthine(IBMX)/insulin
826
827 **Figure 4: MARCH5 modulation in 3T3-L1 adipocytes alters metabolic gene**
828 **expression and cellular metabolism.** Control (shLuc) and MARCH5-KD (shMARCH5)
829 3T3-L1 adipocytes were analysed for (A-D) gene expression using qPCR analysis,
830 presented as fold-change from control. (E) Pseudo-coloured confocal image of
831 mitochondrial morphology in control (shLuc) and MARCH5-KD adipocytes using
832 MitoTracker Deep Red staining (X600). Right panels are enlargements of cell areas
833 depicted by white squares in left panels. (F) Quantification of mitochondrial networks in
834 control (shLuc) and MARCH5-KD adipocytes, measured as the mean number of
835 mitochondrial branches, using MiNA and Fiji Image software. (G) Western blots for
836 Mfn2, as a measure of mitochondrial fusion and MARCH5 activity, in control (shLuc)
837 and MARCH5-KD adipocytes at day 0 and day 6 post differentiation. (H) Oil Red-O
838 staining for neutral lipid deposition photomicrographs of MARCH5-KD and control
839 (shLuc) adipocytes at low (40x) and high (200x) magnification. (I) Quantification of
840 neutral lipid staining from Oil-Red O imaging. (J) Glucose uptake in MARCH5-KD and
841 control (shLUC) 3T3-L1 adipocytes. (K) *Pdk4* gene expression in MARCH5-KD and
842 control (shLUC) 3T3-L1 adipocytes throughout differentiation (day -3 to day 6) (L)
843 Respirometry data from MARCH5-KD and control (shLuc) adipocytes using the
844 Seahorse Flux analyser measuring the oxygen consumption rate (OCR) including basal,
845 FCCP uncoupled respiration (UCP), and ATP linked respiration, and (M) extra cellular
846 acidification rate (ECAR) as a proxy measure of glycolysis and glycolytic capacity.
847 Gene expression analysis from differentiated 3T3-L1 cells infected with adenoviruses for

(N) *Gfp* and (O) *March5*. (P) *Pdk4* gene expression in MARCH5 overexpressing and control (GFP) 3T3-L1 adipocytes. Seahorse analysis on control (GFP) and MARCH5 overexpressing cells plotting (Q) OCR and (R) ECAR. All values presented as mean±SEM, *p<0.05 vs control (shLuc or GFP Tg).

Figure 5: MARCH5 over expression in white adipose tissue of C57BL/6J mice alters expression of metabolic and mitochondrial genes. C57BL/6J mice at 4 weeks of age received contralateral injections of control (MCS) or MARCH5 AAVs (rAAV6) subcutaneously into developing inguinal fat pads and were fed a HFD for 4 weeks. Bar graphs depicting gene expression in excised control-AAV and MARCH5-AAV subcutaneous fat pads of the same animal for (A) MARCH5, (B) adipogenic genes, (C) mitochondrial fusion and fission genes, (D) apoptosis genes and (E) lipid metabolism genes. All data presented as mean±SEM, *p<0.05 from control (MCS-AAV).

Figure 1

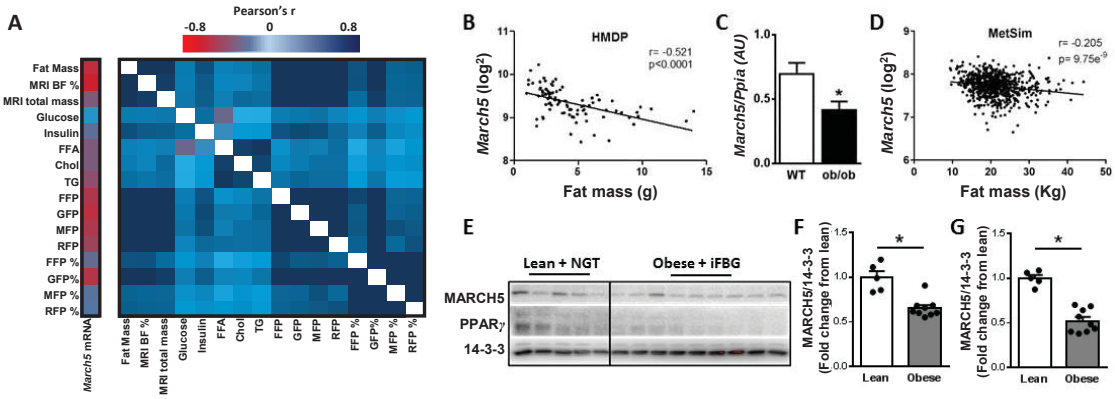
A
Pearson's r
-0.8
0
0.8
Fat Mass
MRI BF %
MRI total mass
Glucose
Insulin
FFA
Chol
TG
FFP
GFP
MFP
RFP
FFP %
GFP%
MFP %
RFP %
March5 mRNA
B
HMDP
r= -0.521
p<0.0001
March5 (log2)
Fat mass (g)
C
March5/Ppia (AU)
WT
ob/ob
D
MetSim
r= -0.205
p= 9.75e-9
March5 (log2)
Fat mass (Kg)
E
Lean + NGT
Obese + iFBG
MARCH5
PPARγ
14-3-3
F
MARCH5/14-3-3 (Fold change from lean)
Lean
Obese
G
MARCH5/14-3-3 (Fold change from lean)
Lean
Obese

Figure 2

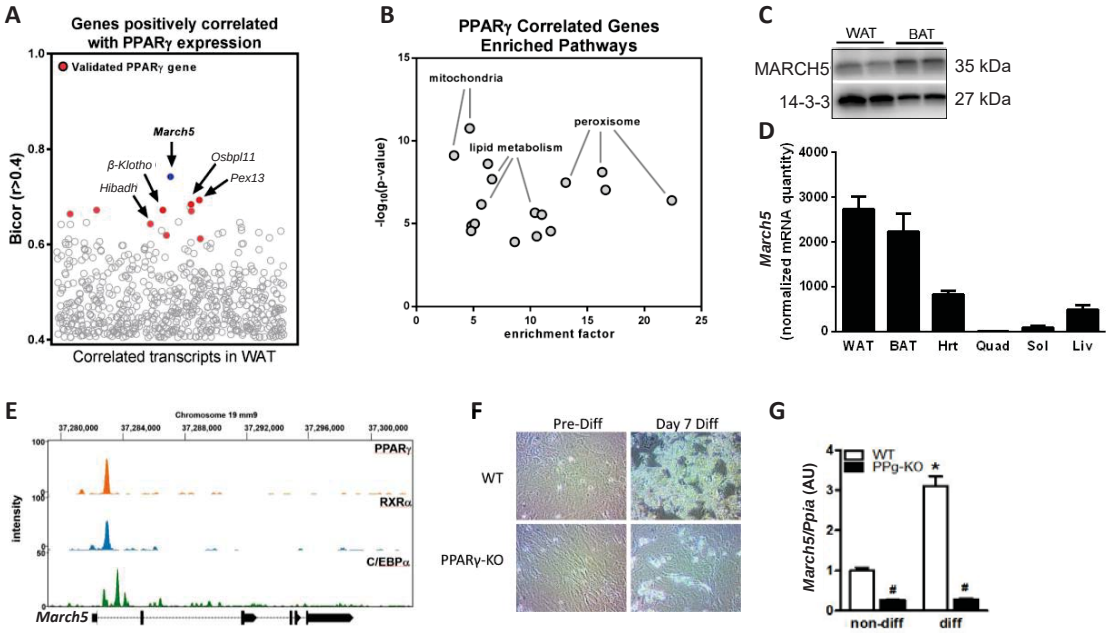
A
Genes positively correlated with PPARγ expression
Validated PPARγ gene
March5
β-Klotho
Osbpl11
Pex13
Hibadh
Bicor (r>0.4)
Correlated transcripts in WAT
B
PPARγ Correlated Genes Enriched Pathways
mitochondria
lipid metabolism
peroxisome
-log10(p-value)
enrichment factor
C
WAT
BAT
MARCH5
14-3-3
35 kDa
27 kDa
D
March5 (normalized mRNA quantity)
WAT
BAT
Hrt
Quad
Sol
Liv
E
Chromosome 19 mm9
PPARγ
RXRα
C/EBPα
intensity
March5
F
Pre-Diff
Day 7 Diff
WT
PPARγ-KO
G
WT
PPg-KO
March5/Ppia (AU)
non-diff
diff

Figure 3

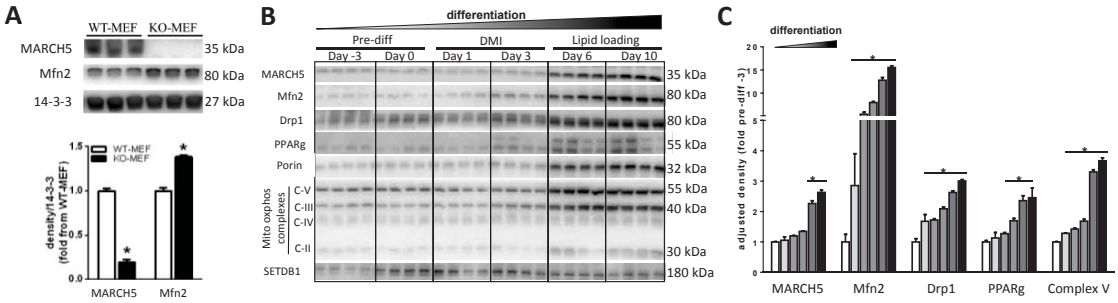
A
WT-MEF
KO-MEF
MARCH5
Mfn2
14-3-3
35 kDa
80 kDa
27 kDa
density/14-3-3 (fold from WT-MEF)
MARCH5
Mfn2
B
differentiation
Pre-diff
DMI
Lipid loading
Day -3
Day 0
Day 1
Day 3
Day 6
Day 10
MARCH5
Mfn2
Drp1
PPARg
Porin
Mito oxphos complexes
C-V
C-III
C-IV
C-II
SETDB1
35 kDa
80 kDa
80 kDa
55 kDa
32 kDa
55 kDa
40 kDa
30 kDa
180 kDa
C
differentiation
adjusted density (fold pre-diff -3)
MARCH5
Mfn2
Drp1
PPARg
Complex V

Figure 4

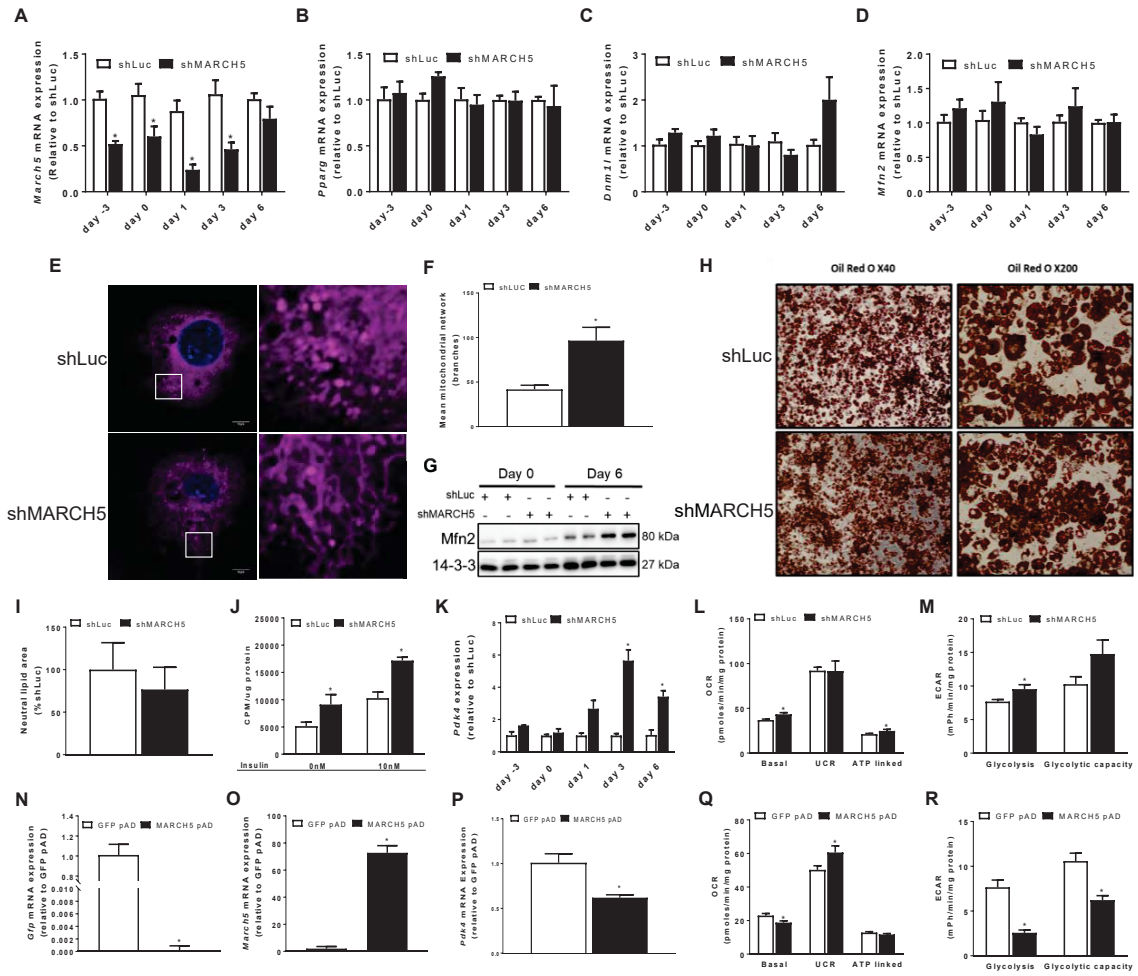
A
B
C
D
shLuc
shMARCH5
March5 mRNA expression (Relative to shLuc)
Pparg mRNA expression (relative to shLuc)
Dnm1l mRNA expression (relative to shLuc)
Mfn2 mRNA expression (relative to shLuc)
day -3
day 0
day 1
day 3
day 6
E
F
G
H
Mean mitochondrial network (branches)
Day 0
Day 6
Mfn2
14-3-3
80 kDa
27 kDa
Oil Red O X40
Oil Red O X200
I
J
K
L
M
Neutral lipid area (%shLuc)
CPM/ug protein
Insulin
0nM
10nM
Pdk4 expression (relative to shLuc)
OCR (pmoles/min/mg protein)
Basal
UCR
ATP linked
ECAR (mPh/min/mg protein)
Glycolysis
Glycolytic capacity
N
O
P
Q
R
GFP pAD
MARCH5 pAD
Glp mRNA expression (relative to GFP pAD)
March5 mRNA expression (relative to GFP pAD)
Pdk4 mRNA Expression (relative to GFP pAD)

Figure 5

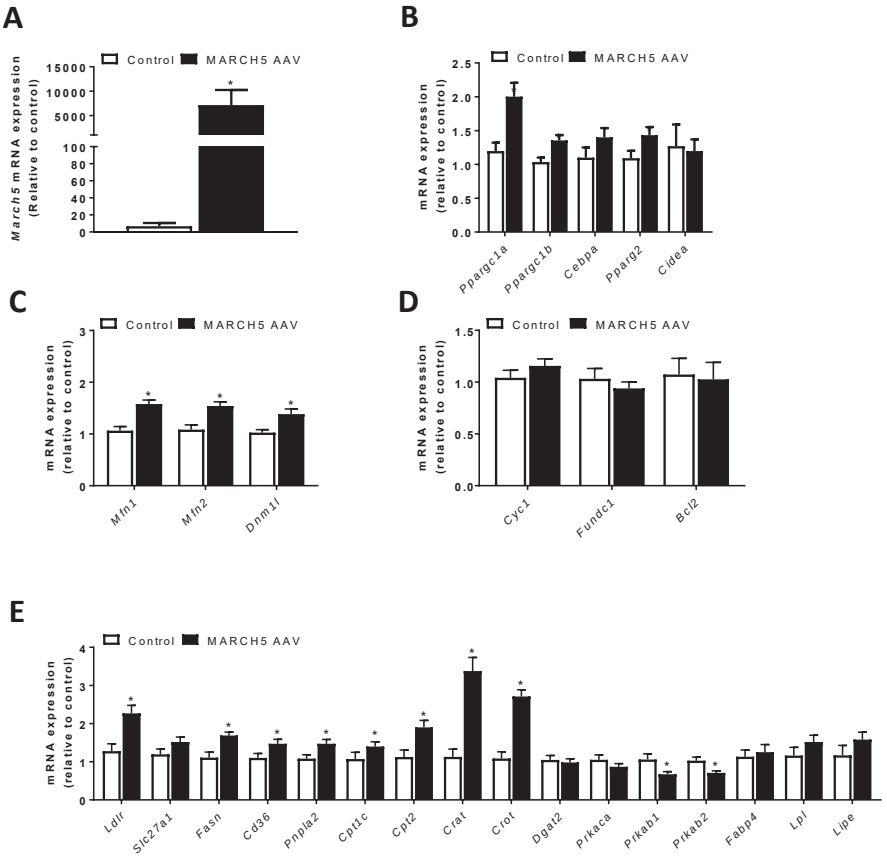
A
Control
MARCH5 AAV
March5 mRNA expression (Relative to control)
15000
10000
5000
100
80
60
40
20
0
B
Control
MARCH5 AAV
mRNA expression (relative to control)
2.5
2.0
1.5
1.0
0.5
0.0
Ppargc1a
Ppargc1b
Cebpa
Pparg2
Cidea
C
Control
MARCH5 AAV
mRNA expression (relative to control)
3
2
1
0
Mfn1
Mfn2
Dnm1l
D
Control
MARCH5 AAV
mRNA expression (relative to control)
1.5
1.0
0.5
0.0
Cyc1
Fundc1
Bcl2
E
Control
MARCH5 AAV
mRNA expression (relative to control)
4
3
2
1
0
Ldlr
Slc27a1
Fasn
Cd36
Pnpla2
Cpt1c
Cpt2
Crat
Crot
Dgat2
Prkaca
Prkab1
Prkab2
Fabp4
Lpl
Lipe